Improved Spice Models of Aluminum Electrolytic Capacitors for Inverter Applications

Sam G. Parler, Jr.
Cornell Dubilier
140 Technology Place
Liberty, SC 29657

Abstract — **Impedance modeling of aluminum electrolytic capacitors presents a challenge to design engineers, due to the complex nature of the capacitor construction. Unlike an electrostatic capacitor, an electrolytic capacitor behaves like a lossy coaxial distributed RC circuit element whose series and distributed resistances are strong functions of temperature and frequency. This behavior gives rise to values of capacitance, ESR (effective series resistance), and impedance that vary by several orders of magnitude over the typical frequency and temperature range of power inverter applications. Existing public-domain Spice models do not accurately account for this behavior. In this paper, a physics-based approach is used to develop an improved impedance model that is interpreted both in pure Spice circuit models and in math functions.**

I. INTRODUCTION

Existing public-domain models of aluminum electrolytic capacitor impedance vary from the least sophisticated, fixed series RLC, to models that add some parallel leakage components as well as temperature and frequency variation to the series resistance component. Actual devices exhibit changes in capacitance and resistance that may vary by orders of magnitude from their nominal values and even from values predicted by existing models. See Figure 1. Capacitor users are often mystified by such things as why the resonant frequency changes with temperature, or why the resonant frequency is often higher than predicted by $f_R = [2\pi \text{sqrt}(LC)]^{-1}$.

The goal of this paper is to present the development of a physics-based model, to show how such a model can be implemented in Spice, and to demonstrate its effectiveness in more accurately predicting capacitor behavior in power electronics circuits such as inverters.

II. MODEL COMPONENTS

The proposed model is a direct result of the construction of the capacitor. An aluminum electrolytic capacitor comprises a cylindrical winding of an aluminum anode foil, an aluminum cathode foil, and papers that separate these two foils. See Figure 2. The anode foil is generally highly etched for a micro-scopic-to-macroscopic surface area enhancement of a factor on the order of 100. For the purposes of this paper it will be assumed that the anode etch pattern is cylindrical. See Figure 3. The anode foil is electrochemically anodized in a bath of hot electrolyte. This process grows alumina (aluminum oxide) onto the surface of the pits at a ratio of about 1.2 nm/V. The anodization voltage is generally 20 to 50% higher than the rated voltage, depending on the temperature and life rating. Since for a plate capacitor the capacitance

$$C = \varepsilon_0 \varepsilon_R A / d \qquad (1)$$

where the relative dielectric constant ε_R is a fairly large value of about 9, the surface area A is very large due to the etch enhancement, and thickness d is very thin due to the high field
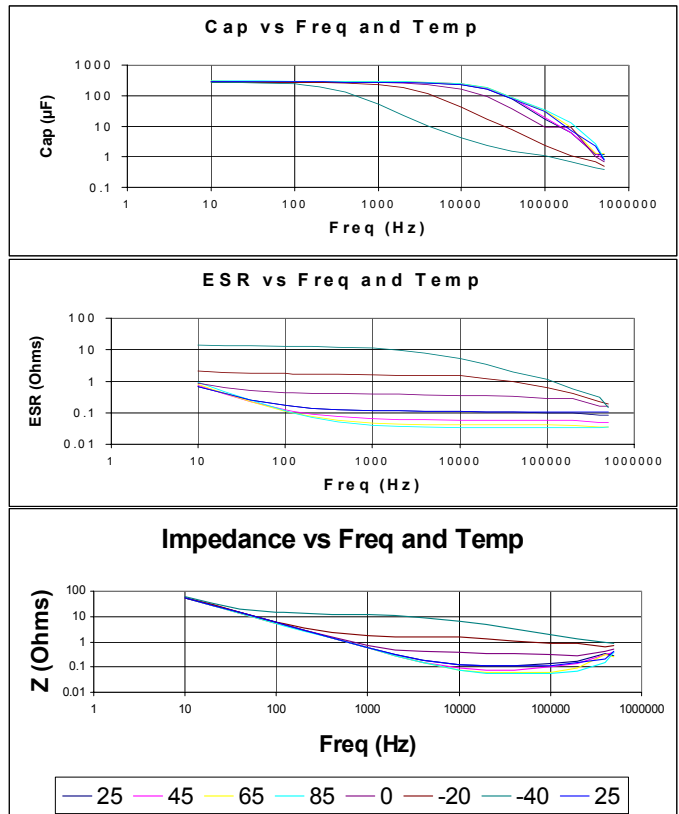

Figure 1. Typical aluminum electrolytic capacitor impedance variation with temperature and frequency.

strength. The capacitance C is enormous compared to that achieved with most other technologies, and hence offers some advantages that may overcome its non-ideal properties.

The cathode foil is usually only ¼ of the thickness of the anode (25 µm instead of 100 µm) and is not usually anodized. The cathode foil may be thought of as a current collector, but it has a large capacitance, which is electrically in series with the anode. The papers may be natural or synthetic, and there are many types and densities. The foils are contacted by aluminum tabs which are generally cold-welded at various positions along the length of the foil. The tabs extend outside the winding and are attached to aluminum terminals.

The dielectric is the aluminum oxide, and one side is contacted by the remaining aluminum of the anode upon which it is grown. The other side of the dielectric is contacted by the electrolyte, which conducts to the cathode. The papers serve as a wick to hold the electrolyte between the foils, and to provide a barrier to prevent the foils from actually touching each other. The electrolyte is formulated not only to conduct current ionically, but also to repair or seal off any defective areas in the anode dielectric. Thus the electrolyte readily provides oxygen to repair any leaky sites. The electrolyte also readily contributes protons, which is good for conduction to the cathode. But if the capacitor is reverse-biased, these protons are too small to be blocked by the aluminum oxide, and cause the dielectric to conduct. Hence the device is polar with protic electrolytes.

Impedance is the ratio (both magnitude and phase) of applied AC voltage to the resulting AC current flow. The voltage is applied to the terminals, and the current flows in from the positive terminal, through the positive tabs to areas on the anode foil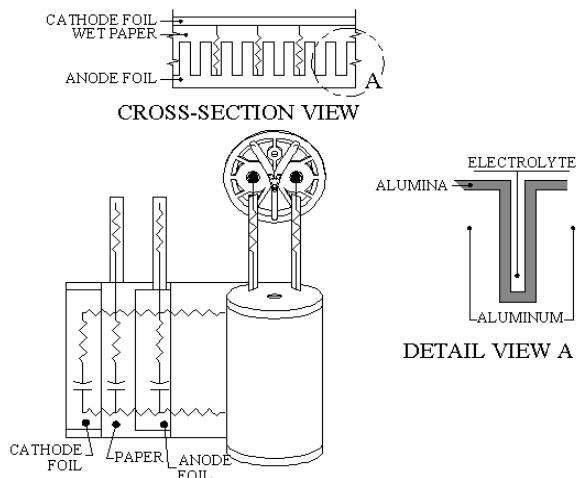 where the tabs are attached. The current branches out from the tabbed areas of the foil to the surrounding areas of the foil, decreasing linearly with the distance from the tab. The current flows up to the surface of the dielectric, inducing a matching flow on the other side of the dielectric which induces ionic motion in the electrolyte that continues to conserve the current flow, which is collected at the cathode where again the current flows electronically to the cathode tab sites to the cathode terminal, completing the circuit. See Figure 4.

From this description of the AC current flow path, the following may be inferred. Inductance might arise from three areas: the loop formed by the terminals and tabs outside of the winding, any offset between the positive and negative current collection areas where the anode and cathode tabs contact the winding, and the etch tunnel inductance. We will show that only the first of these is significant. The total series resistance comprises six terms: 1. terminal resistance, 2. tab resistance, 3. foil resistance, 4. paper-electrolyte resistance, 5. dielectric resistance, and 6. tunnel-electrolyte resistance. Any contact resistance between these elements is assumed to be included in the element resistance. The capacitance stems primarily from the dielectric coating along the deeply etched tunnels, not from the macroscopic foil surface. Let us consider each of these elements in turn.

It can be demonstrated (by placing the anode and cathode tabs several turns apart instead of the usual 1/3-turn apart) that even gross tab misalignment causes only moderate increase in the series inductance. This is because the effective anode-cathode separation area is so small that most of the magnetic flux is cancelled. Likewise, tall capacitor windings (wide foils) do not have significantly more inductance that short windings. Once the tabs enter the active area of the windings, the current

Figure 2. Aluminum electrolytic capacitor construction determines its impedance characteristics.
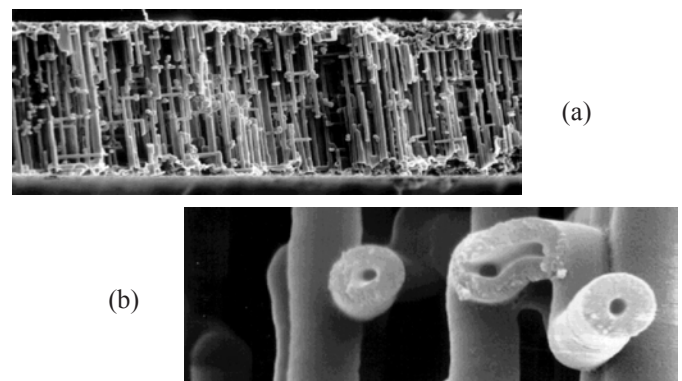

(a)

(b)

Figure 3. Typical anode foil etch pattern and anodization result in high capacitance distributed along electrolyte-filled pores. (a) Edge of 100 µm thick anode foil with aluminum removed, revealing the alumina dielectric. (b) Close-up of dielectric tunnels with 200 nm diameter opening.

2

path quickly changes from a loop to a stripline. Capacitor manufacturers usually incorporate multiple tab pairs on capacitors of diameter greater than 25 mm. But this is done to lower the effective foil resistance, not the inductance. There is some improvement of the inductance, but most of this effect is due an effective increase in the gauge of tab loop.

It is straightforward to show that although the characteristic impedance of the etch tunnels individually are significant (often greater than 10 ohms), the tunnel length of <100 µm leads to noninductive frequency response to above 100 MHz [1].

From this discussion it is concluded that the only significant contributor to the capacitor's series inductance is the tab loop configuration. Knowing this, some manufacturers have used special construction where the anode and cathode tabs are laid atop one another with electrical insulation between. For example, the Cornell Dubilier type 350 uses this technique to achieve a 5 nH total series inductance in a 25 mm diameter plug-in capacitor. Epcos recently presented a paper on a similar concept in a screw-terminal capacitor[2].

The effective series inductance is thus dominated by the loop area from the terminals and tabs outside of the active winding. Heavier gauge tab material and multiple tab sets lower the inductance to some degree. When the tab width is much less than the loop dimensions, we may estimate the loop inductance by modifying an expression found in Grover [3] for a rectangle of circular wire of radius R by substituting $R=$sqrt(wd/π) into

$$L = \mu_0[x\ \ln(2x/R) + y\ \ln(2y/R) + 2\text{sqrt}(x^2+y^2) - x\ \sinh^{-1}(x/y) - y\ \sinh^{-1}(y/x) - 1.75(x+y)]\ /\ \pi \quad (2)$$

where w and d are the tab width and thickness, and x and y are
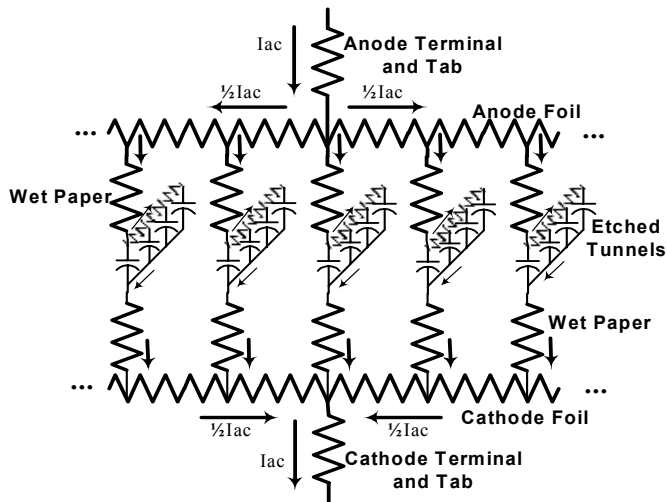

Figure 4. Path of AC current flow through the tabs, foils, dielectric, and electrolyte in an aluminum electrolytic capacitor.

the tab loop width and length. This equation estimates that a tab loop 50 mm × 50 mm with tab width of 9 mm and total tab thickness of 5 mm will have an inductance of 82 nH. Halving the tab thickness increases the inductance by only 14 nH.

A tall capacitor may have slightly higher inductance than a shorter capacitor with the same winding diameter and tab configuration, but this effect is quite small since the current along the tab falls off rapidly once the tab enters the capacitor winding. Typical series inductance values of radial and screw-terminal capacitors are about 1-2 nH/mm terminal spacing. This value does not vary significantly with temperature or frequency, so this portion of the impedance modeling is simple.

The ESR from the terminals and tabs is simple to model from the material conductivity and geometry. Since the current falls off linearly from each tab location as it conducts along the length of the foils, it is straightforward to show that the effective aluminum foil resistance is inversely proportional to the square of the number of tab pairs, provided that the tabs are equally spaced and optimally placed. We have

$$R_{FOIL} = R_F\ /\ 12n^2 \quad (3)$$

where R_F is the resistance (anode plus cathode) from one end of the foils to the other end and n is the number of tab pairs. Naturally these three elements have a slight positive temperature coefficient since the materials are mostly aluminum. There is little frequency variation below 100 kHz, and above 100 kHz this resistance exhibits skin effect, increasing as the square root of frequency.

The bulk electrolyte-paper resistance R_{SP} can be calculated from the geometry (inter-foil spacing) and the electrolyte resistivity, but since the paper's nonconductive cellulose structure interrupts the electrolyte, there is a paper factor that must be used [4]. This factor is not only a function of the paper density, but also of the fiber geometry and orientation, as well as interaction with the electrolyte (wetting). Generally this factor is best measured empirically in a wet cell. R_{SP} varies with temperature but not much with frequency except at temperatures below -20 ºC, where an sudden drop in ESR with increasing frequency is often observed due to dielectric dispersion associated with the colloidal properties of the paper [5]. This temperature dependence is accounted for by variations in the ionic mobility of the ionogens in the electrolyte, which is heavily influenced by the electrolyte viscosity. Generally R_{SP} decreases dramatically as the temperature increases. Most paper-electrolyte systems drop in resistance by 40-80% as the temperature is increased from 25 ºC to 85 ºC.

There are other effects which arise from the paper-electrolyte system. There is a large capacitance C_P associated with the wet paper and chemical double layers at the electrolyte-foil interfaces. This capacitance is in series with the dielectric and is generally so large that it can be neglected. At high frequency-resistivity products (such as high frequencies and/or temperatures below 0 ºC), this capacitance rolls off rapidly with increasing frequency. There is a parallel resistance R_P coupled with the paper capacitance C_P. At high frequencies C_P decreases with the fR_P product[5], meaning that the dielectric loss of the paper capacitance increases with frequency. This effect is not directly modeled in this paper, but an approximate method to account for this effect is mentioned later.

The AC resistance of dielectrics was observed over a century ago to be approximately inversely proportional to frequency over a very broad frequency range. The constant of proportionality between this resistance and the capacitive reactance is known as the dissipation factor, or DF_{OX}, and is approximately 0.015 for anodic alumina, making it a lossy dielectric. DF_{OX} is defined as $\tan(\delta)$, where δ is the angle by which the voltage departs from a 90º ideal phase shift when a sinusoidal current is applied, regardless of frequency. This leads to the conclusion that the energy cycled through the dielectric has a loss that occurs in fixed proportion to the constant DF_{OX}, no matter at what rate (frequency) the energy is stored and removed. DF_{OX} usually has a positive temperature coefficient, though it is modest. This effect can be seen from the crossing slopes of the low-frequency ESR curves of Figure 1. Therefore we have

$$R_{OX}(f,T) = DF_{OX} \times C_T^{T\text{-}298} / 2\,\pi\,f\,C \qquad (4)$$

where C_T is the temperature coefficient, T is the temperature (K). Below some frequency, this term will dominate the ESR. If $R_{ND} \equiv ESR - R_{OX}$ is the frequency-invariant (at these low frequencies of interest), non-dielectric resistance, at room temperature the frequency below which R_{OX} will dominate is

$$f = DF_{OX} / 2\,\pi\,C\,R_{ND}\ . \qquad (5)$$

Of the six elements of ESR that we are considering, only the dielectric resistance R_{OX} is not an ohmic resistance in series with the dielectric. R_{OX} is the one element that causes the terms "ESR" to be used instead of just "SR." R_{OX} is actually a loss internal to the dielectric, and thus does not come into play directly to affect the capacitor's RC time constant. The remainder of the total resistance, R_{ND}, is physically in series with the dielectric.

Finally let us consider the tunnel ESR along with the tunnel capacitance (which accounts for about 99% of the total capacitance, the balance of which arises from the unpitted regions of macroscopic foil surface) since these two parameters are coupled. The tunnels act as a distributed RC circuit element. For a general treatment of the tunnel impedance let us consider a coaxial etch tunnel coated with the alumina dielectric. High-conductivity aluminum contacts the outside of this dielectric, and the electrolyte contacts the inside. The cathode views the impedance Z_{TUN} of the tunnel through the electrolyte at the tunnel opening. It is known that the input impedance of such a construction can be derived from the general expression for the impedance of an unterminated (open-ended) transmission line [6], viz.

$$Z_{TUN} = \text{sqrt}(z/y)\ \coth[\lambda\ \text{sqrt}(yz)] \qquad (6)$$

where λ is the tunnel length, z is the series impedance per unit length and y is the shunt admittance per unit length of the tunnel. Neglecting the resistance of the aluminum, the series impedance per unit length is the resistance of the electrolyte plus the inductive reactance per unit length, which we will show can also be neglected. The resistance of the tunnel per unit length is

$$r(T) = \rho(T) / \pi\,R_I^2 \qquad (7)$$

where R_I is the inner radius of the tunnel. The inductive reactance per unit length is

$$x(f) = j\,\mu_0\,f\,\ln(R_O/R_I) \qquad (8)$$

where j is $\sqrt{-1}$, μ_0 is the magnetic permeability of free space and R_O is the outer diameter of the dielectric tunnel. Since R_I is generally about 1 μm and only one order of magnitude smaller than R_O, and electrolyte resistivity $\rho(T)$ (which is a very strong function of the temperature T) is at least 50 Ωcm, we see that r is at least 10^7 times larger than x at frequencies f below 100 MHz, so that x may be neglected, and therefore

$$z \approx r\ . \qquad (9)$$

Since the low-frequency tunnel capacitance is

$$C_{TUN,DC} = 2\,\pi\,\varepsilon_R\varepsilon_0\,f\,\lambda / \ln(R_O/R_I)\ , \qquad (10)$$

the shunt admittance per unit length of the dielectric tunnel is

$$y = j4\pi^2\,\varepsilon_R\varepsilon_0\,f / \ln(R_O/R_I) \qquad (11)$$

where ε_0 is the electric permittivity of free space and ε_R is the relative dielectric constant, about 9. Substituting (9) and (11) into (6), we may obtain the tunnel impedance Z_{TUN} at the open-

4

ing of the tunnel. Next, we may obtain the frequency response of the tunnel resistance as

$$R_{TUN}(f,T) = \text{Re}\{Z_{TUN}\} \tag{12}$$

and the tunnel capacitance frequency response as

$$C_{TUN}(f,T) = 1 / j\omega \, \text{Im}\{Z_{TUN}\} \tag{13}$$

where $\omega = 2\pi f$ is the angular frequency. For an actual capacitor, we may estimate the total number of tunnels n_{TUN} as the nominal device capacitance C_{NOM} divided by the low-frequency tunnel capacitance $C_{TUN,DC}$:

$$n_{TUN} = C_{NOM} / C_{TUN,DC} . \tag{14}$$

This scaling factor allows straightforward computation of the total contributions from the etched dielectric tunnels to the total device capacitance and ESR.

$$C_T = \frac{n_{TUN}(e^{2\beta\sqrt{\omega}} - 2e^{\beta\sqrt{\omega}}\cos\beta\sqrt{\omega} + 1)}{\alpha \, (2e^{\beta\sqrt{\omega}}\sin\beta\sqrt{\omega} + e^{2\beta\sqrt{\omega}} - 1)\sqrt{\omega}} \tag{15}$$

and

$$R_T = \frac{\alpha \, (e^{2\beta\sqrt{\omega}} - 2e^{\beta\sqrt{\omega}}\sin\beta\sqrt{\omega} - 1)}{n_{TUN}(e^{2\beta\sqrt{\omega}} - 2e^{\beta\sqrt{\omega}}\cos\beta\sqrt{\omega} + 1)\sqrt{\omega}} \tag{16}$$

where $\alpha = \text{sqrt}(r/2c)$ and $\beta = \lambda\text{sqrt}(2rc)$.

It is interesting to note that the low-frequency tunnel resistance is only one-third of the electrolyte channel resistance $r\lambda$ from one end of the tunnel to the other. As for the effective foil resistance, this is because the AC current increases linearly from the tunnel end to its opening, so that if the total injected current is I_{AC} and x is the position along the tunnel from the end to the opening, we have

$$P = I_{AC}{}^2 R_{EFF} = \int_{x=0}^{\lambda} (I_{AC}x/\lambda)^2 \, r dx \ = r\lambda I_{AC}{}^2/3 \tag{17}$$

These equations lead to the characteristic backwards-S curve of C vs f, and as the frequency increases beyond 100 kHz, the impedance approaches zero magnitude at -45º phase angle.

This AC frequency response of the capacitor impedance, capacitance, and ESR is sufficient to predict the capacitor behavior when the frequency content of the capacitor ripple current is known (or can be measured or calculated). In addition, because this model is physically based, it is also powerful enough to be useful in transient solutions and even when the capacitor response itself determines the circuit current to a large extent, such as low-temperature strobe applications and self-discharge

("crowbar") simulations. In these cases the Laplace transform is used by replacing ω in the equations above with $-js$. Such techniques generally lead to the diffusion equation [7]. Although there are a few known analytical solutions to such problems with simple boundary conditions, in general a partial differential equation solver is indicated.

III. COMPLETE MODEL

Assembling the components developed in the preceding section, we have

$$ESR = R_{TERM}(T) + R_{TABS} (T) + R_{FOIL}(T) + R_{SP}(T)$$
$$+ R_{OX}(f,T,C) + R_T(f,T) \tag{18}$$

$$C = C_T(f,T) \ // \ [\kappa C_{NOM}] \tag{19}$$

and inductance value of simply L. Skin effect is omitted from the metallic resistance (first three terms) of *ESR*, but could easily be added as begin at 100 kHz and increase as the square root of frequency. C_{NOM} denotes the nominal device capacitance. Equation (19) indicates that a small portion κ (about 1%, $\kappa = 0.01$) of the device capacitance is not distributed in the etched dielectric tunnels. Note that the term R_{OX} technically should use the value of C from equation (19) as its input, not the nominal capacitance. Knowing the variation of resistivity with temperature, some of the effects of the spacer paper, and the etch tunnel geometry has allowed us to put these elements together into a predictive model that agrees well with the experimental results. See Figure 5 and compare to Figure 1.

IV. INTERPRETING BRIDGE READINGS

Much confusion arises from interpretation of capacitor impedance data from capacitance bridges. Generally, a high-quality capacitance bridge can make capacitance and ESR measurements from about 10 Hz to around 1 MHz with an AC bias of up to 1V or 100 mA. This is done with connection leads
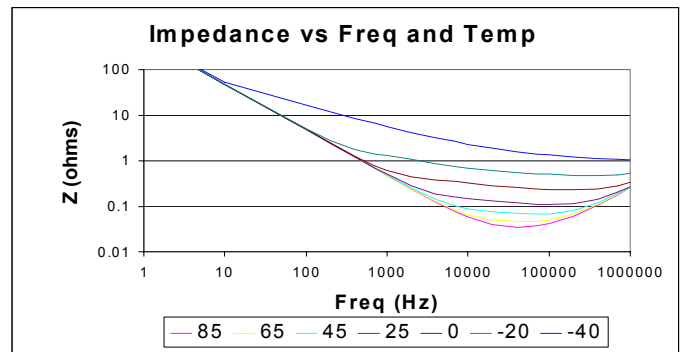

Figure 5. Impedance model results for capacitor of Figure 1.

5

configured in a 4-terminal "Kelvin" connection to reduce the effect of the leads. Usually there is a calibration procedure for the bridge that incorporates an open circuit and a closed-circuit lead connection.

The bridge's 4-terminal connection works by injecting the sinusoidal test current through one pair of terminals, and sensing the voltage magnitude and phase shift (relative to the injected current) with the other pair. *The impedance vector (magnitude and phase) is what the bridge always measures, but the way this information is interpreted and displayed is* often user-selectable among the following: *Cs, Cp, Rs, Rp,* ESR, *Ls, Lp, |Z|,* θ, *DF, Q, |Y|, Gp, Xs, Bp.* If the bridge user selects *Cs* and *Rs* (or equivalently, ESR) to be displayed, the bridge has no choice but to display the impedance and phase information *as if it were an ideal capacitor in series with an ideal resistor.* The bridge simply has no means of segregating the inductive and capacitive impedance contributions. Therefore, just below self-resonance, the capacitance will appear to be increasing, and above resonance, it will appear to be negative. At resonance, the capacitance is at a singularity, tending simultaneously toward positive and negative infinity. See Figure 6.

It is a simple matter to infer the actual capacitance since the series inductance is truly in series and is frequency- and temperature-invariant. Letting C_A denote the actual capacitance, C_B denote the bridge-indicated capacitance, and L_S denote the series inductance, we have

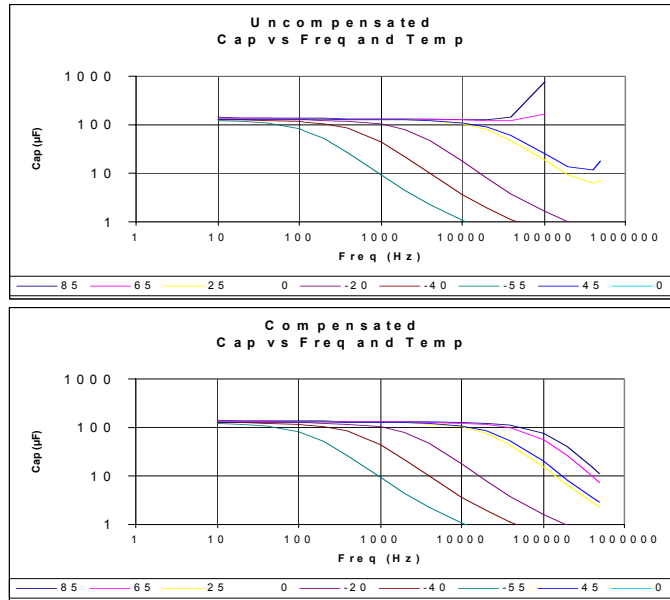$$(\omega C_B)^{-1} = (\omega C_A)^{-1} - \omega L_S \tag{20}$$

Figure 6. Uncompensated and compensated capacitance data. Effect of 30 nH series inductance affects bridge capacitance.

so that

$$C_B = C_A (1 - \omega^2 C_A L_S)^{-1} \tag{21}$$

and

$$C_A = C_B (1 + \omega^2 C_B L_S)^{-1} . \tag{22}$$

Figure 6 also shows the transformed data, which unveils the actual capacitor behavior that the inductance obfuscates. It is important to remember that the series inductance is in the capacitor's equivalent circuit and cannot be neglected.

Since the capacitance varies strongly with frequency and temperature, and the series inductance is constant, it should be no surprise that the resonant frequency of an aluminum electrolytic capacitor varies with temperature. Because the capacitance rolloff usually begins below a frequency of $[2\pi \text{sqrt}(LC_{NOM})]^{-1}$, the actual resonant frequency may be considerably higher than what is predicted based on the nominal capacitance.

This paper is focussed on aluminum electrolytic capacitors with a wet electrolyte. A note is made here regarding aluminum electrolytic capacitors constructed with a solid polymer "electrolyte." Actually, the solid polymer material used in surface mount aluminum electrolytic capacitors conducts electronically rather than ionically, so it is not an electrolyte. The electrical conductivity of these materials is very high, so that the tunnel rolloff of capacitance and ESR is often extended beyond 1 MHz. There is no viscosity-temperature effect and little variation of conductivity with temperature, so the capacitance, ESR, and impedance curves show little temperature variation.

The relationship between impedance magnitude |Z| and phase θ and the indicated bridge capacitance and ESR are as follows:

$$|Z| = \text{sqrt} (R_S^2 + (\omega C_B)^{-2}) \tag{23}$$

$$\theta = \text{Tan}^{-1}((\omega R_S C_B)^{-1}) \tag{24}$$

$$R_S = |Z|\cos\theta \tag{25}$$

$$C_B = -|Z|\sin\theta \tag{26}$$

V. SPICE IMPLEMENTATIONS

There are several ways to implement the model in Spice and PSpice. The best method may depend on the specific version of Spice being used. For example, to model the etch tunnel distributed *RC* characteristics, OrCAD PSpice 9 offers a lossy transmission line model TLOSSY (denoted by letter T) while

6

other versions may have URC (uniform distributed *RC*) model or the newer LTRA (lossy transmission line). Other techniques include Analog Behavioral Modeling (ABM) or Macromodeling using the equations developed in this paper, or even their Laplace domain equivalents. IntuSoft's IsSpice version 4 and later allows frequency-dependent resistances to be modeled. Because there are so many different modeling techniques to model these circuits mathematically, no one technique is presented here. But the basic equations have been developed and are readily implemented. A more general implementation is to use pure PSpice basic circuit elements.

Pure PSpice elements may be used in an *RC* ladder configuration. This has been done for solid tantalum capacitors by Kemet[8], where the capacitance rolloff is emphasized by exponentially backloading the capacitance but using constant resistance values, since apparently the tunnel resistance is small compared to the rest of the ESR or is offset by other effects. For high-frequency AC, small-signal, and most transient analysis, especially when the total capacitor power loss needs to be modeled, we have found that the Kemet model can be adapted to work quite well for aluminum electrolytic capacitors. Apparently the etch tunnel ESR rolloff is often offset by an increase in the dispersion (parallel loss) of the paper-electrolyte-interface system at high frequencies.

We have found that with proper selection of the *R* and *C* values (exponentially back-loaded resistance and capacitance), both the impedance and phase (thus the capacitance and ESR) of the etch tunnels can be reproduced to within about 1% accuracy with a 5-stage *RC* over a very broad frequency range. This may allow more accurate transient response predictions in some situations like pulse-discharge modeling. For example, consider the 270 µF capacitor whose impedance sweep is shown in Figure 1. Its 25 ºC high-frequency ESR is just over 100 milliohms. When this capacitor is actually pulse-discharged into a low-resistance load, the voltage drop at the capacitor terminals after the peak current is reached at 4 µs is about 30 volts when the current is 500 amps, resulting in an effective series resistance value of about half of that measured on the impedance bridge. This result agrees with the transient model, but not the small-signal AC model.

There are additional refinements that can be added to the model presented here, depending on what the goals and ranges of the Spice simulation are. For example, the skin effect can be modeled with a couple of parallel *RL* stages connected in series with each other and with the rest of the circuit. Dielectric loss effects can be added with several more *RC* stages beyond the tunnel *RC* stages. (Recommended total capacitance about 10% of C_{NOM}, slightly front-loaded; exponentially backloaded resistance that scales with DF_{OX}/C_{NOM}.) The capacitor's zener effect (when taken above its rated voltage) can be modeled as a zener diode in series with a low resistance value. Temperature coefficients can be added to the resistances (positive for the metallic elements and negative for the electrolytic elements). Figure 7 shows a summary of a comprehensive equivalent circuit with these optional elements.
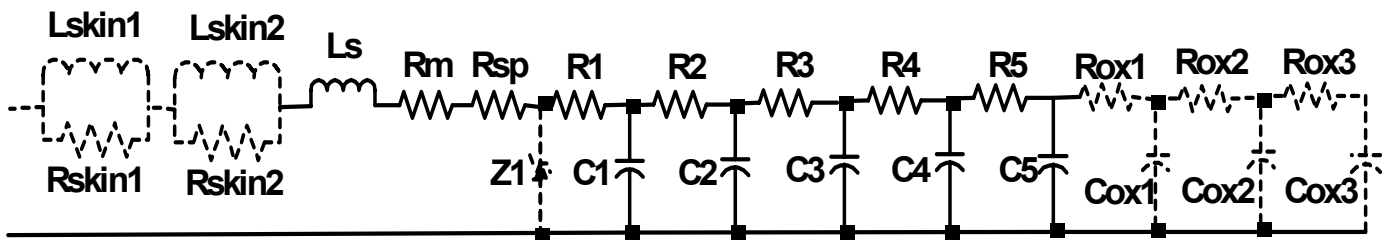

Figure 7. General model of aluminum electrolytic capacitor using pure PSpice elements. Optional skin-effect stages, Zener clamping element, and dielectric loss stages are shown in dashed lines. This model is suitable for AC or Transient analysis, depending on the selection of values for R1-R5.

7

VI. SOME RESULTS

If the *R* and *C* are properly chosen for a given frequency and temperature of interest, in many cases a series *RLC* model is actually not a bad model. The problem is, that to know what value of *R* and *C* to use, one must have measured or simulated the values of the inductance, capacitance, and ESR. The equations developed in this paper can be used to determine lumped *R*, *L*, and *C* values. Figure 8 shows several model examples, contrasting the series *RLC* model to the model of Figure 7.

VII. CONCLUSIONS

We have explored the issues and theory behind impedance modeling of aluminum electrolytic capacitors and have developed and presented a model that has simulation and predictive value over a broad range of frequencies and temperatures, both in steady-state AC and in transient simulations.

The limitations of this model involve the capacitance and dispersion effects of paper-electrolyte and of chemical double-layer. This is worked around by noting that these effects often approximately offset the rolloff of the etch tunnel resistance with frequency. These issues and appropriate models will be the focus of future work.

REFERENCES

[1] Peekema, R. M. and Beesley, J. P., "Factors affecting the impedance of foil-type electrolytic capacitors." Electrochem. Techn. vol. 6, no. 5-6, May-June 1968, pp. 166-72.

[2] Will, N. F. and Fischer, E., "New electrolytic capacitors with low inductance simplify inverter." IEEE Industry Applications Society Meeting, Rome, 2000.

[3] Grover, F. W., Inductance Calculations: Working Formulas and Tables. Dover Publications, New York, 1946, p. 60.

[4] Alwitt, R. S., "Electrical conductivity of paper and cellophane in aqueous and nonaqueous electrolyte solutions." Electrochem. Techn. vol 6., no. 5-6, May-June 1968, pp. 172-178.

[5] Alwitt, R. S., "Contribution of spacer paper to the frequency and temperature characteristics of electrolytic capacitors." J. Electrochem. Soc., vol. 116, no. 7, July 1969, pp.1023-1027.

[6] De Levie, R., "On porous electrodes in electrolyte solutions-IV." Electrochem. Acta, vol. 9, 1964, pp. 1231-45.

[7] Kahng, A. B. and Muddu, S., "Delay analysis of VLSI interconnections using the diffusion equation model." Proc. ACM/IEEE Design Automation Conf., June 1994, pp. 563-569.

[8] Prymak, J. D., "SPICE modeling of capacitors." 15th Annual Capacitor and Resistor Technology Symposium, Components Technology Institute Inc., Huntsville, AL, 1995.
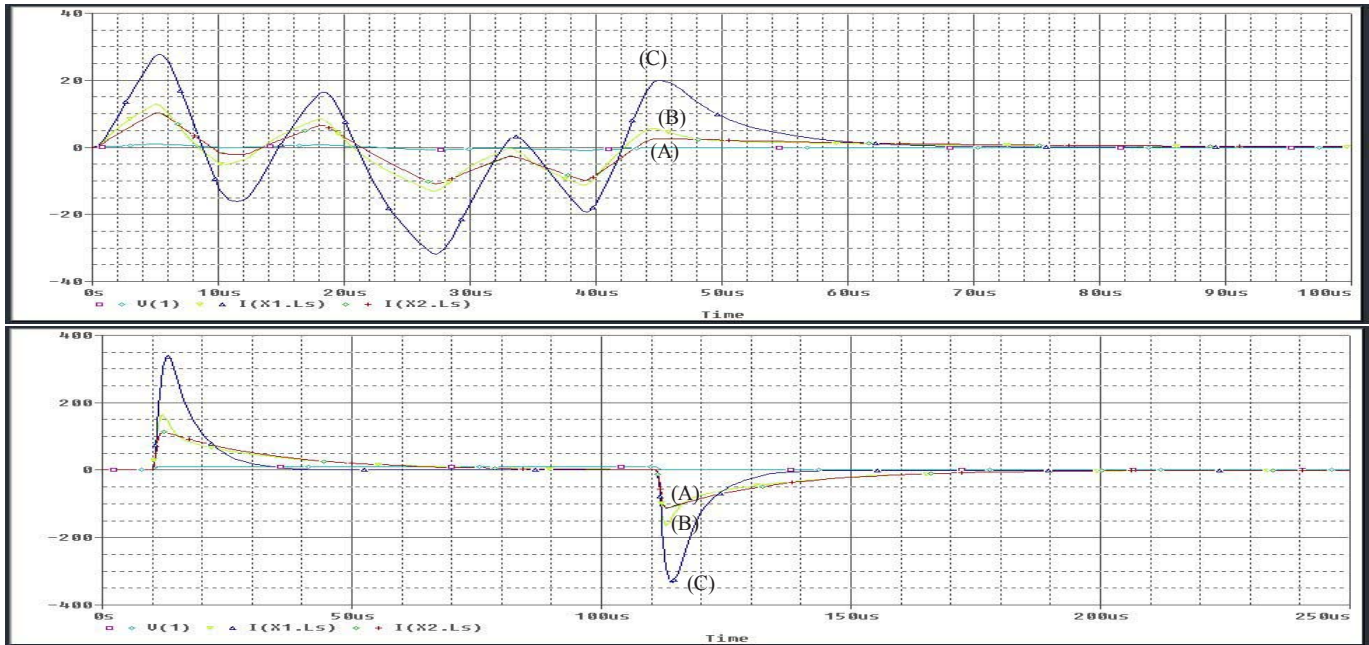
Figure 8. Model results of transient simulation of transient model compared to lumped RLC model. The top simulation shows the current response to a piecewise linear voltage impressed at the capacitor terminals. The bottom simulations shows the current response to a voltage step. In both figures, trace (A) refers to the RLC model with 25 ºC values, trace (B) refers to the transient model at 25 ºC, and trace (C) refers to the transient model at 85 ºC. OrCAD PSpice version 9.2 was used in these simulations.

8